Pomiary Automatyka Robotyka, ISSN 1427-9126, R. 29, Nr 3/2025, 119–127, DOI: 10.14313/PAR_257/119

Verification of the die Temperature of a SiC Transistor Based on the Thermal Imaging and Machine Learning

Krzysztof Dziarski
Poznań University of Technology, Institute of Electric Power Engineering, Piotrowo 3A, 60-965 Poznań, Poland
Arkadiusz Hulewicz
Poznań University of Technology, Institute of Electrical Engineering and Electronics, Piotrowo 3A, 60-965 Poznan, Poland

Abstract: The article presents a method for the automatic verification of the thermograms of the transistor packages, enabling the differentiation between those in which the die temperature is correct and those in which it is too high. This method is based on an indirect thermographic measurement of the transistor die temperature. The paper describes a measurement methodology that provides a reliable temperature assessment, based on simulations using the Finite Element Method (FEM). A transistor operating in pulsed mode (switching at a specific frequency, rather than in the active state) was used. The procedure for determining the coefficients required for these simulations is also presented. Additionally, the article includes an algorithm for analyzing thermograms of the investigated transistor packages and the results of this analysis, which allow for distinguishing components operating at the correct and excessive temperatures.

Keywords: thermography, artificial neural network, convolutional neural network

Nomenclature

ε	emissivity	Pr	Prandtl number
σ	Stefan-Boltzmann constant	R_{DS}	drain-source resistance
	dynamic air viscosity equal	$R_{\mathrm{Pt\ 1000}}$	Pt 1000 resistance
c	specific heat	T	temperature
C_{GS}	gate-source capacitance	T_a	ambient temperature
C_{th}	thermal capacity	T_c	the case temperature
e, f	coefficients	T_j	the die temperature
Gr	Grashof number	T_{js}	die temperature determined by simulation
h_r	radiation coefficient		
h_c	convection coefficient	$T_{\mathrm{Pt\ 1000}}$	Pt 1000 temperature
I_{DS}	drain-source current	q_v	power density dissipated in the die
I_{DSS}	saturation current		
$I_{\mathrm{Pt\ 1000}}$	Pt 1000 current	q	heat flux
$(k)\lambda$	thermal conductivity	V_{th}	threshold voltage
Nu	Nusselt number	V_{DS}	drain-source voltage
P_c	total power applied to the wall	$V_{\mathrm{Pt\ 1000}}$	Pt 1000 voltage
P_j	power dissipated in die		

Autor korespondujący:
Krzysztof Dziarski, krzysztof.dziarski@put.poznan.pl

Artykuł recenzowany
nadesłany 02.07.2025 r., przyjęty do druku 08.09.2025 r.

1. Introduction

As the drain-source current (I_{DS}) increases, the temperature of the transistor's semiconductor structure (die) also rises. An increase in switching frequency likewise leads to a rise in die temperature [1, 2]. This occurs because more frequent switching results in higher switching losses. *Consequently*, the rising die temperature causes an increase in the temperature of the transistor's package. Based on this relationship, the die temperature can be indirectly determined. In practice, it is crucial to quickly detect whether the die temperature exceeds permissible limits. It is also important to assess whether there is a risk of the damage to the semiconductor structure.

The excessive die temperature shortens the operational lifespan of the transistor and increases the risk of damage to internal connections (bond wires). A rise in die temperature also affects the transistor's parameters. For example, the threshold voltage V_{th}, the saturation current I_{DSS}, and the gate-source capacitance C_{GS} all change. Additionally, the shape of the drain current I_D versus drain-source voltage V_{DS} cha-

racteristic is altered. If the die temperature exceeds a critical threshold, the permanent damage to the semiconductor structure may occur [3].

There are two methods for monitoring the die temperature. The first is the direct method, which involves placing a temperature sensor directly on the die structure [4]. The second is the indirect method, which can be divided into two categories [5].

The first category is the indirect electrical method. It involves determining the die temperature based on a parameter that depends on that temperature. This parameter is called a Thermal Sensitive Parameter (TSP). A detailed description of these methods can be found in the JEDEC (EIA/JESD51-1) standards [16].

The second category is the indirect thermal method. It consists of two stages. First, the case temperature of the transistor (T_c) is measured. Then, based on a known relationship $T_j = \mathrm{f}(T_c)$, the die temperature (T_j) of the semiconductor structure is determined. This category includes the indirect infrared thermographic measurement of temperature. In this case, T_c is measured using a thermographic camera. This type of measurement does not require damaging the transistor package. It is also safe for the user, as there is no risk of the electric shock.

The relationship $T_j = \mathrm{f}(T_c)$ can be determined using the numerical methods, including the Finite Element Method (FEM). The indirect thermographic method enables the evaluation of the die temperature without physical contact. However, it requires reading the temperature from the thermogram and using the transfer function $T_j = \mathrm{f}(T_c)$ [6–9].

In practice, the useful method would be one that automatically classifies thermograms, distinguishing between those that show a transistor with a normal die temperature and those in which the die temperature is too high. To this end, a study was conducted with the aim of developing a method for automatic classification of the thermograms of the transistor package, based on the temperature of the semiconductor die.

2. Methodology

2.1. The measurement system

As the part of the experimental setup, a C2m0280120d transistor from Wolfspeed (Durham, NC, USA) was used. This SiC-based device features the maximum drain-source voltage of 1200 V, the continuous drain current I_{DS} of 11 A at 25 °C, and an on-state resistance R_{DS} of 280 mΩ – nominal specifications [17].

In order to develop a method for the automatic classification of the thermograms depicting the transistor package based on the temperature of the semiconductor die, it was necessary to create a thermogram database. This required knowing the die temperature of the transistor at the moment the package thermogram was captured. For this purpose, an indirect thermographic temperature measurement was proposed. The first part of the applied method involved performing a reliable measurement of the transistor package temperature.

To avoid the issue of unknown emissivity of the transistor package, a reference marker was applied to its surface using Velvet Coating 811-21, which is characterized by a well-defined emissivity coefficient (ε) in the range 0.970 to 0.975 within the temperature interval of 237.15 K to 355.15 K. The uncertainty of the emissivity value was estimated to be 0.004 [10].

Adjacent to the marker, the Pt 1000 temperature sensor in an SDM 0603 package (Royal Ohm, Chachoengsao, Thailand) [18] was attached directly to the surface of the epoxy mold compound that encapsulates the transistor die and base plate. The sensor was positioned in a location estimated to be directly above the die. Placing the Pt 1000 sensor next to the marker allowed for the verification of the reliability of the thermographic temperature measurement.

The sensor was bonded using WLK 5 thermal adhesive (Fischer Elektronik, Lüdenscheid, Germany), known for its thermal conductivity of 0.836 W/m · K in the temperature range of 217.15 K to 422.15 K [19].

The electrical connections were made using a four-wire measurement setup, including a current source, voltmeter and ammeter. Due to the small form factor of the sensor package, thin wires with a diameter of 0.3 mm were employed. To avoid self-heating effects, a measurement current of 100 µA was applied. The preliminary tests confirmed that this current level does not introduce the significant thermal error. The resistance $R_{\mathrm{Pt\ 1000}}$ was calculated by dividing the measured voltage $V_{\mathrm{Pt\ 1000}}$ by the applied current $I_{\mathrm{Pt\ 1000}}$. The discussed measurement system is shown in Figure 1.

The transistor assembly was positioned beneath a thermographic camera, maintaining a 33 mm gap between the transistor and the camera lens. For this study, a FLIR E50 thermographic camera (Flir, Wilsonville, OR, USA) [15] equipped with a Close 2× macro lens was used. Measurements were carried out under the steady-state thermal conditions.

Preliminary observations revealed that the temperature of the epoxy mold compound differed from the ambient temperature by more than 80 mK. Moreover, the successive measurement points confirmed that the temperature of the mold compound consistently exceeded this threshold. These findings justified the use of a thermographic system employing an uncooled microbolometer detector array, which was deemed appropriate for the purposes of this study.

The area of the epoxy mold compound observed during measurement covered a surface of 20 mm by 21 mm. The FLIR E50 thermographic camera utilized in the experiment is equipped with an uncooled microbolometer sensor array with a native resolution of 240 × 180 px [21]. According to the Close-up 2 × lens specifications [22], the Instantaneous Field of View (IFOV) corresponding to this setup is 87 µm.

Given this IFOV value, it is possible to capture more than nine individual detector fields (pixels) across the observed region, confirming that the spatial resolution of the imaging system is adequate for the analysis. Prior to conducting measurements, the camera's calibration was verified against a reference blackbody source (IRS Calilux IP, AT – Automation Technology, Bad Oldesloe, Germany) to ensure the accuracy of the thermal readings [23].

The thermographic camera and the transistor assembly were placed inside a custom-built enclosure constructed from plexiglass, with the internal dimensions of 40 cm × 30 cm × 30 cm.

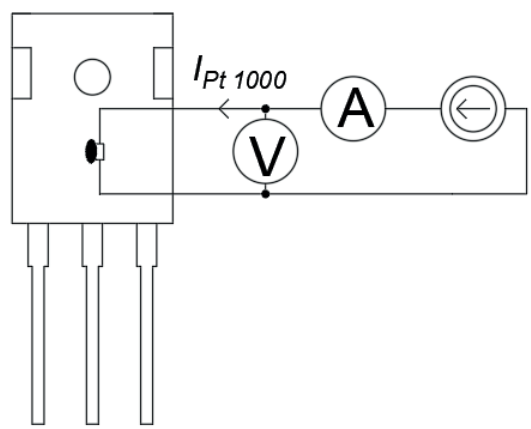

Fig. 1. The temperature measurement setup using a Pt 1000 sensor
Rys. 1. Układ pomiarowy do pomiaru temperatury za pomocą czujnika Pt 1000

The inner walls of the container were lined with polyurethane-based black foam. Due to the structure of its open-cell pores, which resemble the behavior of a blackbody cavity, this material exhibits a high emissivity value of approximately $\varepsilon = 0.94$ [11]. This design effectively shielded the measurement setup from the external thermal influences and significantly reduced the internal reflections.

To adjust the distance d between the lens of the thermographic camera and the surface of the epoxy mold compound, the camera was mounted on a tripod integrated with a stepper motor. This motorized positioning system allowed for precise control of d, managed by a Siemens S7-1200 1214DC/DC/DC programmable logic controller (Siemens, München, Germany) [24]. The desired distance was set using a Siemens KTP 700 Basic PN touchscreen interface [25]. A view of the complete measurement setup is shown in Figure 2.

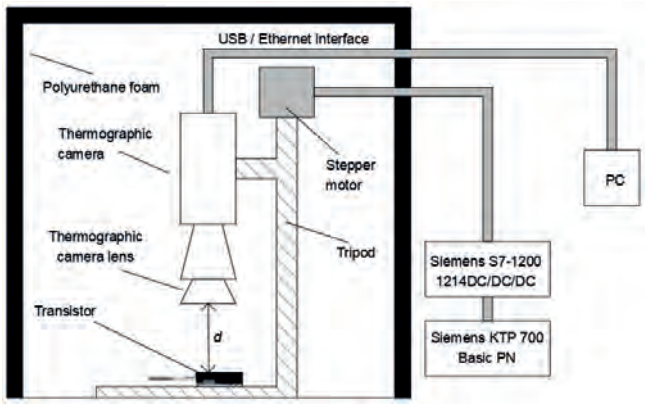

Fig. 2. The measuring system
Rys. 2. Układ pomiarowy

2.2. Finite element method and boundary conditions

An essential stage in the process of the indirect thermographic temperature measurement is identifying the correlation between the die temperature and the case temperature. This correlation can be determined through numerical simulations. A commonly used approach for this purpose is the Finite Element Method (FEM). In this method, the analyzed domain – where the temperature distribution is to be assessed – is divided into a finite number of tetrahedral elements.

The equation 1 expresses the heat transfer along the x-axis between two specific points [12]:

$$-q_v = k \cdot \frac{\partial^2 T}{\partial x^2} - c_{th} \cdot \frac{\partial T}{\partial t} \tag{1}$$

where q_v is the power density dissipated in the die in W/m^3, c_{th} is the volumetric thermal capacity in J/(m^{3}K), and T is the temperature.

Under steady-state conditions, the equation 1 simplifies to the form shown in the equation 2 [12]:

$$q = -\lambda \cdot \frac{\partial T}{\partial x} \tag{2}$$

where q is the heat flux in W/m^2.

By applying the method of the separation of the variables and integrating the equation 2, the time constant can be obtained using the boundary conditions specified in the equation 3.

$$\begin{aligned} &\text{for} \quad x = 0 \rightarrow T = T_1 \\ &\text{for} \quad x = x_k \rightarrow T = T_2 \end{aligned} \tag{3}$$

Once the time constant has been determined and it is assumed that the heat flux q has fully traversed the wall, the equation 3 can be rearranged into the form presented in the equation 4.

$$T_1 - T_2 = x_k \cdot \frac{P_c}{k \cdot \lambda} \tag{4}$$

where P_c is the total power applied to the wall in W and S in m^2 is the area of the wall penetrated by q in W/m^2.

To ensure the accurate simulations using the Finite Element Method (FEM), it is essential to define both the radiation coefficient h_r and the convection coefficient h_c. The value of h_r can be calculated using the equation 5.

$$h_r = \sigma \cdot (T_c + T_a) \cdot (T_c^2 + T_a^2) \tag{5}$$

The convection coefficient h_c characterizes the rate of heat transfer by convection per unit area and time. Accurately determining h_c is difficult due to its dependence on the multiple variables, including the object's geometry, the structural complexity and the surface temperature. In this work, h_c was approximated using similarity theory related to transport phenomena. The relationships between the key physical parameters were described using dimensionless numbers such as the Nusselt, Grashof, and Prandtl numbers. For flat surfaces, the convection coefficient can be calculated using the formula presented in the equation 6 [15].

$$h_c = \frac{Nu \cdot \lambda}{L} \tag{6}$$

The Nusselt number can be expressed using the equation 7 [15]:

$$Nu = e(G_r \cdot P_r)^f \tag{7}$$

where e and f are dimensionless coefficients, the values of which depend on the shape and the orientation of the analyzed surface and the product $P_r \cdot G_r$. P_r (–) is the Prandtl number, G_r is the Grashof number.

The coefficients e and f depend on the product of the Grashof and Prandtl numbers, as well as on the orientation of the surface in question and the type of airflow – whether laminar or turbulent. The suitable values for these coefficients are provided in Table 1 [13].

Tab. 1. Values of the coefficients *e* and *f*
Tab. 1. Wartości współczynników *e* i *f*

Shape	G_rP_r	e_{lab}	f_{lam}	e_{turb}	f_{turb}
Vertical flat wall	10^9	0.59	0.25	0.129	0.33
Upper flat wall	10^8	0.54	0.25	0.14	0.33
Lower flat wall	10^5	0.25	0.25	NA	NA

The Prandtl number can be obtained using the equation 8 [13]:

$$P_r = \frac{c \cdot \psi}{\lambda} \tag{8}$$

where c is the specific air heat equal to 1005 in $J \cdot kg^{-1} \cdot K^{-1}$ in 293.15 K, ψ is the dynamic air viscosity equal to 1.75×10^{-5} in $kg \cdot m^{-1} \cdot s^{-1}$ in 273.15 K.

Grashof number is obtained from the equation 9 [13]:

$$G_r = \frac{\alpha \cdot g \cdot (T_c - T_a) \cdot \rho_d^3 \cdot L^3}{\psi^2} \tag{9}$$

where α is a coefficient of expansion equal to 0.0034 in K^{-1}, g is the gravitational acceleration of 9.8 in $m \cdot s^{-2}$, ρ_d is air density equal to 1.21 in $kg \cdot m^{-3}$ in 273.15 K.

2.3. Classification of thermal images of SiC transistors

Thermograms showing the transistor case with a die at a proper temperature and those with an overheated die can be distinguished. For the automatic classification of the thermograms, a Convolutional Neural Network (CNN) architecture was selected [14, 15]. This type of artificial neural network is specifically designed to process the image data. Its fundamental component is the convolutional layer, whose task is to detect the image features such as edges, lines, curves, and texture. These layers can also be trained to recognize color-related patterns if the color is present in the input data. An important part of the CNN architecture is the ReLU (Rectified Linear Unit) activation layer. The presence of this layer enables, among other things, the modeling of more complex relationships and helps to mitigate the issues such as the vanishing gradient problem.

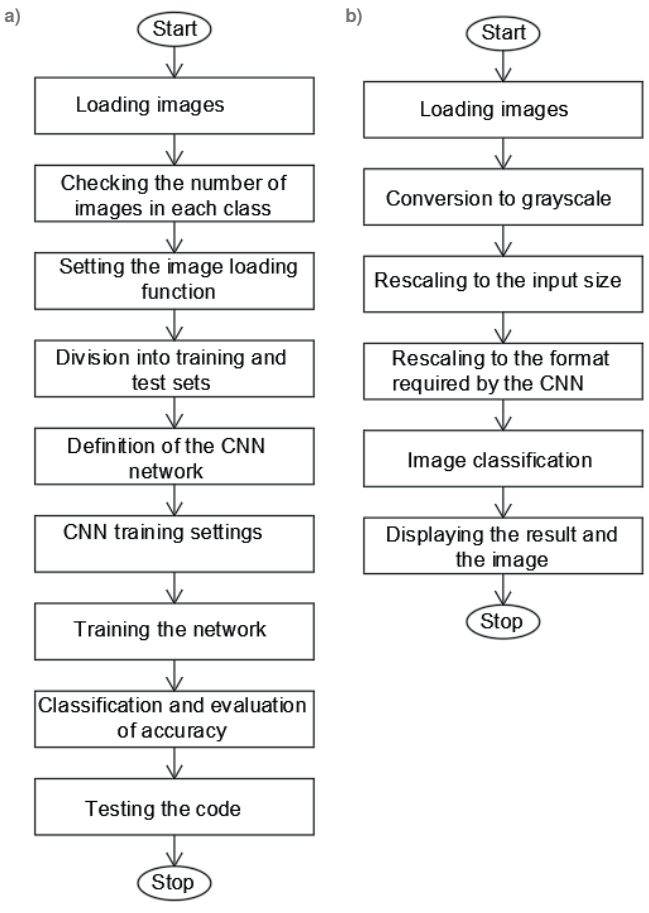

Fig. 3. a) The algorithm for data loading, creating and training the neural networks and classifying thermograms, b) the algorithm illustrating the loading and classification of a thermogram. The training was carried out exclusively on the CPU, without the use of GPU acceleration or parallel computing. No data augmentation was applied. The average processing time per epoch was approximately 10 seconds.

Rys. 3. a) Algorytm ładowania danych, tworzenia i trenowania sieci neuronowych oraz klasyfikacji termogramów, b) algorytm ilustrujący ładowanie i klasyfikację termogramu. Uczenie przeprowadzono wyłącznie na CPU, bez wykorzystania akceleracji GPU ani obliczeń równoległych. Nie zastosowano augmentacji danych. Średni czas przetwarzania jednej epoki wynosił około 10 sekund.

Tab. 2. Structure of the defined neural network

Tab. 2. Struktura zdefiniowanej sieci neuronowej

No.	Layer	Type
1	Input	Image Input
2	Convolution	Conv2D
3	Batch Normalization	Batch Norm
4	Activation	ReLU
5	Max Pooling	MaxPooling2D
6	Convolution	Conv2D
7	Batch Normalization	Batch Norm
8	Activation	ReLU
9	Max Pooling	MaxPooling2D
10	Convolution	Conv2D
11	Batch Normalization	Batch Norm
12	Activation	ReLU
13	Fully Connected Layer	Fully Connected
14	Softmax	Softmax
15	Classification Layer	Classification Output

In the conducted study, MATLAB was used to create and train the convolutional neural network, along with the Deep Learning Toolbox and Image Processing Toolbox packages. The Deep Learning Toolbox is responsible for creating and training the neural networks, while the Image Processing Toolbox is used for loading, processing and analyzing images.

A database of 48 thermograms was used for the study. Twenty of them depicted the transistor package with an excessively high die temperature, while the remaining twenty-eight showed the package with an appropriate die temperature. The first stage of the study involved loading the images with the labels and verifying the number of thermograms in each class. The thermograms were divided into two classes: those with proper die temperature and those with improper die temperature. Next, the input file size was selected, and a loading function was defined. The thermograms were then split into a training set and a test set in an 80/20 ratio, meaning 20 % of the thermograms were placed in the test set, and the remaining 80 % in the training set. After defining the CNN architecture, the training options were set. Only 10 epochs were sufficient to train the neural network. Finally, the classification and the code testing were carried out. Figure 3a presents the algorithm used for data loading, the neural network construction and training, and thermogram clas-

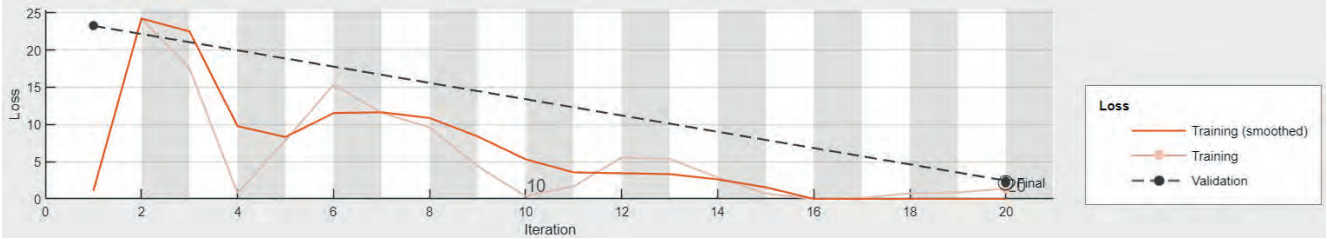

Fig. 4. An example loss curve
Rys. 4. Przykładowa krzywa strat

sification. Figure 3b illustrates the procedure for loading and classifying an individual thermogram.

The designed Convolutional Neural Network (CNN) had a layered structure composed of the sequentially connected elements. The input layer accepted color images in JPG format, stored in the RGB color model. Immediately after the input layer, the first convolutional block was applied, consisting of a convolutional layer with 8 filters of size 3 × 3 (with 'same' padding), a batch normalization layer, a ReLU activation function, and a max pooling layer with dimensions 2 × 2 and a stride of 2. The second convolutional block included a convolutional layer with 16 filters of size 3 × 3 (also with 'same' padding), followed by batch normalization, ReLU activation, and a max pooling layer with the same parameters as in the first block. The third block used 32 filters of size 3 × 3 and also included a batch normalization layer and a ReLU activation function. At the end of the architecture, a fully connected layer was placed, generating two outputs corresponding to the classes "correct" and "incorrect". These outputs were converted into probabilities using the softmax layer and the final classification was performed by the classification layer, based on the highest predicted probability. The applied architecture is presented in Table 2. An example loss curve is shown in Figure 4.

3. Results

The research work began with the acquisition of a series of 48 thermograms. For this purpose, the measurement system shown in Figure 2 was used. During the experiments, the I_{DS} current was set successively to 0.25 A, 0.5 A, and 1.5 A. For each I_{DS} value, the transistor switching frequency f was varied. An example thermogram is shown in Figure 5.

Next, the measurements of the internal dimensions of the transistor case were carried out. For this purpose, the transistor package was opened. To calibrate the microscope prior to the measurements, a calibration slide was used. As a result, it was possible to create a three-dimensional model.

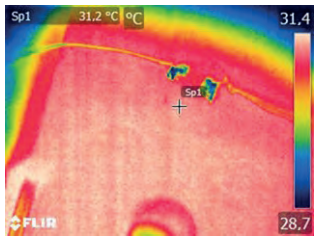

Fig. 5. Example thermogram for I_{DS} = 0.25 A, f = 10 kHz
Rys. 5. Przykładowy termogram dla I_{DS} = 0,25 A, f = 10 kHz

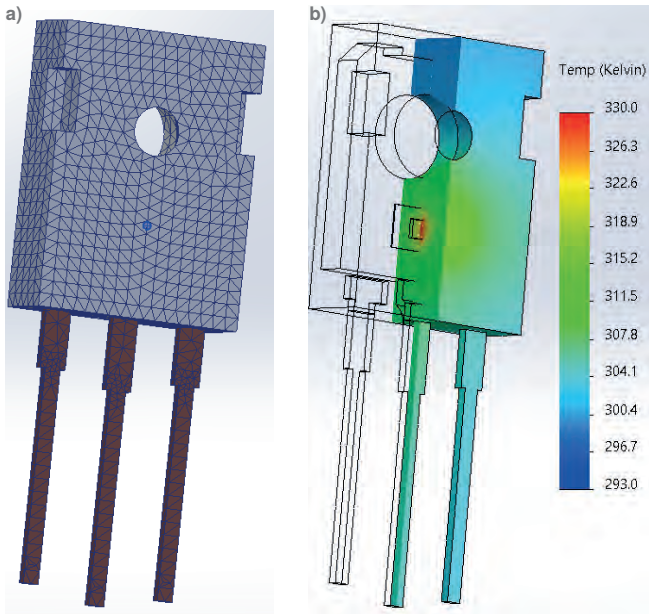

Fig. 6. a) The completed model with the mesh and the point where the results were recorded, b) the cross-section of the element for I_{DS} = 0.25 A, f_t = 100 kHz
Rys. 6. Kompletny model tranzystora z siatką oraz punktem, w którym rejestrowano wyniki, b) przekrój elementu dla I_{DS} = 0,25 A, ft = 100 kHz

The model and the simulation work were carried out using SolidWorks software. The appropriate mesh size was determined by varying the edge length of the mesh cells. Simultaneously, the accuracy of the obtained results and simulation time were monitored. The sample results are presented in Table 3. The mesh cell size shown in the last row was selected for use in the simulation.

The completed model with the mesh and the point where the results were recorded is shown in Fig. 6a. Figure 6b presents the cross-section of the element for $I_{DS} = 0.25$ A, $f_t = 100$ kHz.

The materials assigned to the individual components of the model, along with the selected properties, are presented in Table 4.

Based on the simulation work, it was possible to determine the relationship between the die temperature and the case temperature of the transistor. The obtained results are presented in Tables 5–8.

Tab. 3. The size of the mesh elements, the obtained results and the duration of the simulation
Tab. 3. Wymiary elementów siatki, uzyskane wyniki oraz czas trwania symulacji

No.	mesh size	accuracy of obtained result	duration of the simulation
	[mm]	[°C]	[s]
1	2.5	0.5	2
2	1.5	0.3	3
3	0.5	0.1	50
4	1.0	0.1	8

Tab. 4. The materials assigned to the individual components of the model, along with the selected properties [8]
Tab. 4. Materiały przypisane do poszczególnych elementów modelu wraz z wybranymi właściwościami [8]

Internal Structure Component	Material	K [W/m·K]	h_c [–]	ε [–]
Black part of the case	EME 590	0.25	9.5–14.3	0.97
Back part of the case	Copper	400	9.5–14.3	0.23
Semiconductor element	Silicon carbide	150	–	–
Left lead	Copper	400	9.5–14.3	0.09
Internal lead	Copper	400	9.5–14.3	0.09
Right lead	Copper	400	9.5–14.3	0.09
Internal connections	Copper	400	–	–
Grease	Melamine resin	0.2	19.9–29.6	0.97

In order to increase the number of the thermograms in the dataset, the additional thermograms were added. The measured values recorded during their acquisition are shown in Table 8.

Due to the low turn-on and turn-off times of SiC transistors (on the order of 10–12 ns), at an average current $I_{DS} \leq 1.5$ A, the switching losses depend only slightly on frequency. As a result, the junction temperature T_j and the case temperature T_c depend only slightly on the device switching frequency.

After completing the measurements, the obtained thermograms were divided into two classes: the thermograms representing a transistor with a proper die temperature and the thermograms representing a transistor with an improper (too high) die temperature. The first class consisted of 28 thermograms. These were thermograms showing a transistor through which a drain current I_{DS} of 0.25 A and 0.5 A was flowing – Tables 5 and 6, as well as the first two rows of Table 7. The second class included the remaining thermograms – Table 8 and Table 7, rows 3 to 9.

Tab. 5. The measured values of T_c (temperature measurement by the thermographic camera), the measured values of $T_{Pt\,1000}$ (temperature measurement by Pt 1000) and the values of T_{js} (die temperature determined by the simulation) for all values of f_t and I_{DS} = 0.25 A
Tab. 5. Zmierzone wartości T_c (pomiar temperatury kamerą termowizyjną), zmierzone wartości $T_{Pt\,1000}$ (pomiar temperatury czujnikiem Pt 1000) oraz wartości T_{js} (temperatura złącza wyznaczona w symulacji) dla wszystkich wartości f_t i I_{DS} = 0,25 A

No.	f_t	I_{DS}	T_c	$T_{Pt\,1000}$	T_{js}
[–]	[kHz]	[A]	[K]	[K]	[K]
1	1	0.25	311.8	311.5	328.2
2	5	0.25	312.1	311.9	328.6
3	10	0.25	312.1	312.0	328.7
4	50	0.25	312.3	312.2	329.0
5	100	0.25	313.0	312.9	329.9
6	150	0.25	313.8	313.5	331.0
7	200	0.25	314.0	313.7	331.6
8	300	0.25	314.7	314.4	332.4
9	400	0.25	314.7	314.4	332.8
10	500	0.25	314.9	314.6	333.2
11	600	0.25	315.1	315.0	333.2
12	700	0.25	315.2	315.0	333.3
13	800	0.25	315.4	315.2	333.6

Tab. 6. The measured values of T_c (temperature measurement by the thermographic camera), the measured values of $T_{Pt\,1000}$ (temperature measurement by Pt 1000) and the values of T_{js} (die temperature determined by the simulation) for all values of f_t and I_{DS} = 0.50 A
Tab. 6. Zmierzone wartości T_c (pomiar temperatury kamerą termowizyjną), zmierzone wartości $T_{Pt\,1000}$ (pomiar temperatury czujnikiem Pt 1000) oraz wartości T_{js} (temperatura złącza wyznaczona w symulacji) dla wszystkich wartości f_t i I_{DS} = 0,50 A

No.	f_t	I_{DS}	T_c	$T_{Pt\,1000}$	T_{js}
[–]	[kHz]	[A]	[K]	[K]	[K]
1	1	0.50	324.4	324.3	344.6
2	5	0.50	324.8	324.5	345.2
3	10	0.50	324.9	324.8	345.3
4	50	0.50	325.7	325.4	346.4
5	100	0.50	326.5	326.4	347.6
6	150	0.50	327.1	327.0	348.4
7	200	0.50	327.8	327.5	349.4
8	300	0.50	328.1	327.8	349.9
9	400	0.50	328.6	328.3	350.6
10	500	0.50	328.7	328.4	350.7
11	600	0.50	328.6	328.3	350.6
12	700	0.50	328.8	328.5	350.9
13	800	0.50	329.1	329.0	351.3

Next, a neural network was created and trained using the MATLAB environment along with the Deep Learning Toolbox and Image Processing Toolbox. The algorithm presented in Fig. 3a was used. Thermograms were tested randomly using the algorithm shown in Fig. 3b. To verify the final classification results, a confusion matrix was prepared. The classification accuracy was calculated to be 90 %. The confusion matrix is presented in Table 9.

Next, the division of thermograms was modified. The ratio of the training dataset to the testing dataset was set to 50/50. Additionally, the number of the epochs was increased to 12. classification accuracy of 83.33 % was achieved. The confusion matrix is presented in Table 10.

4. Conclusion and discussion

The objective of the conducted work was to develop a method enabling the automatic classification of the thermograms into two categories: those showing a transistor package with a die operating at an appropriate temperature and those with an elevated die temperature. A threshold value of 351.3 K (78.15 °C) was adopted. This value was arbitrarily selected based on the authors' observations. It was necessary to establish this threshold in order to divide the thermograms into two classes – representing either acceptable or excessive die temperatures – for the purpose of training the classification model. For die temperatures not exceeding this value, no malfunction of the transistor was observed. This applies to a transistor operating without a heatsink, under the natural convection conditions and at an ambient temperature (T_a) = 20 °C. When calculating the power dissipated in the transistor die, the conduction, blocking, and switching losses were taken into account.

The obtained thermographic temperature measurement results were verified by comparison with measurements performed using a Pt 1000 sensor (Tables 5–8). Considering the thermographic camera's accuracy of ±2 °C or ±2 % of the reading (whichever is greater), it can be observed that the thermographic temperature measurements of the transistor package are consistent with the results obtained using the Pt 1000 sensor. Additionally, prior to performing the measurements, the thermographic camera's readings were validated using a blackbody reference. Therefore, the thermographic temperature measurement results can be regarded as reliable.

Analyzing the thermograms reveals that the case temperature depends on the die temperature. In the conducted study, the die temperature was determined based on the indirect

Table 7. The measured values of T_c (temperature measurement by the thermographic camera), the measured values of $T_{Pt\,1000}$ (temperature measurement by Pt 1000) and the values of T_{js} (die temperature determined by the simulation) for all values of ft and I_{DS} = 1.00 A

Tab. 7. Zmierzone wartości T_c (pomiar temperatury kamerą termowizyjną), zmierzone wartości $T_{Pt\,1000}$ (pomiar temperatury czujnikiem Pt 1000) oraz wartości T_{js} (temperatura złącza wyznaczona w symulacji) dla wszystkich wartości f_t i I_{DS} = 1,00 A

No.	f_t	I_{DS}	T_c	$T_{Pt\,1000}$	T_{js}
[–]	[kHz]	[A]	[K]	[K]	[K]
1	1	1.00	358.4	358.1	393.2
2	5	1.00	361.5	361.3	397.6
3	10	1.00	364.4	364.1	401.7
4	50	1.00	364.6	364.4	402.0
5	100	1.00	366.7	366.6	405.0
6	150	1.00	367.5	367.3	406.2
7	200	1.00	368.1	367.8	407.0
8	300	1.00	368.0	367.7	406.9
9	400	1.00	368.1	367.9	407.0
10	500	1.00	368.6	368.3	407.7
11	600	1.00	368.3	368.1	407.3
12	700	1.00	368.9	368.7	408.2
13	800	1.00	368.4	368.1	407.4

Tab. 8. The measured values of T_c (temperature measurement by the thermographic camera), the measured values of $T_{Pt\,1000}$ (temperature measurement by Pt 1000) and the values of T_{js} (die temperature determined by the simulation) for all values of f_t and I_{DS}

Tab. 8. Zmierzone wartości T_c (pomiar temperatury kamerą termowizyjną), zmierzone wartości $T_{Pt\,1000}$ (pomiar temperatury czujnikiem Pt 1000) oraz wartości T_{js} (temperatura złącza wyznaczona w symulacji) dla wszystkich wartości f_t i I_{DS}

No.	f_t	I_{DS}	T_c	$T_{Pt\,1000}$	T_{js}
	[kHz]	[A]	[K]	[K]	[K]
1	10	0.25	312.3	312.1	328.5
2	300	0.25	314.6	314.3	332.5
3	1	1.5	384.9	382.5	413.0
4	5	1.5	386.3	383.8	413.7
5	10	1.5	386.4	383.9	413.9
6	50	1.5	386.2	383.7	413.5
7	100	1.5	386.3	383.8	413.7
8	300	1.5	386.4	383.9	413.9
9	500	1.5	386.4	383.9	413.9

Tab. 9. The confusion matrix determined for a training-to-testing dataset ratio of 20/80

Tab. 9. Macierz pomyłek wyznaczona dla stosunku zbioru treningowego do testowego wynoszącego 20/80

–	incorrect	correct
incorrect	3	1
correct	0	6

Tab. 10. The confusion matrix determined for a training-to-testing dataset ratio of 50/50

Tab. 10. Macierz pomyłek wyznaczona dla stosunku zbioru treningowego do testowego wynoszącego 50/50

–	incorrect	correct
incorrect	6	4
correct	0	14

thermographic temperature measurement. It is possible to associate the thermogram (image) with the die temperature. Based on the authors' previous work, it can be concluded that the proposed method of the indirect thermographic temperature measurement provides reliable results.

The thermogram classification using a CNN (Convolutional Neural Network) is feasible and provides reliable results. In the conducted study, the thermograms were divided into a training set and a test set in ratios of 20/80 and 50/50. Analyzing the results presented in Table 9, it can be observed that out of 10 thermograms in the test set, 3 were correctly identified as the thermograms showing a transistor with an excessively high die temperature, 6 thermograms were correctly classified as depicting the transistor case with a proper die temperature and 1 thermogram was incorrectly classified as showing a transistor with a proper die temperature. The overall classification accuracy reached 90 %.

When the thermograms were divided into a training set and a test set in a 50/50 ratio, the test set included 24 thermograms. Of these, 6 were correctly identified as the thermograms showing a transistor with an excessively high die temperature, 14 thermograms were correctly classified as depicting the transistor case with a proper die temperature and 4 thermograms were incorrectly classified as showing a transistor with a proper die temperature. The overall classification accuracy was 83.33 %.

The presented method should be further developed. The results obtained so far should be considered preliminary. In the future, a larger number of thermograms from a wider range of components should be analyzed. The proposed method may prove useful for the rapid real-time analysis of the performance of the electronic components.

The article presents the concept of using a Convolutional Neural Network (CNN) for the classification of the thermograms into two categories: thermograms showing a transistor package with an appropriate die temperature and the thermograms showing a transistor package with an inappropriate die temperature. The presented results are preliminary findings. For this reason, a small dataset consisting of 28 thermograms was used. To perform a proper classification, it is necessary to use a dataset containing several hundred thermograms.

Bibliography

1. Morel C., Rizoug N., *Electro-Thermal Modeling, Aging and Lifetime Estimation of Power Electronic MOSFETs*, "Civil Engineering Research Journal", Vol. 14, No. 1, 2023, DOI: 10.19080/CERJ.2023.14.555879.
2. Morel C., Morel J., *Chaos Anticontrol and Switching Frequency Impact on MOSFET Junction Temperature and Lifetime*, "Actuators", Vol. 14, No. 5, 2025, DOI: 10.3390/act14050203.
3. Lelis A.J., Habersat D.B., Green R., Goldsman N., *Temperature-Dependence of SiC MOSFET Threshold-Voltage Instability*, "Materials Science Forum", Vols. 600–603, 2008, 807–810, DOI: 10.4028/www.scientific.net/msf.600-603.807.
4. Davidson J.N., Stone D.A., Foster M.P., Gladwin D.T., *Measurement and characterization technique for real-time die temperature prediction of MOSFET-based power electronics*, "IEEE Transactions on Power Electronics", Vol. 31, No. 6, 2016, 4378–4388, DOI: 10.1109/TPEL.2015.2476557.
5. Dziarski K., Hulewicz A., Kuwałek P., Wiczyński G., *Methods of Measurement of Die Temperature of Semiconductor Elements: A Review*, "Energies", Vol. 16, No. 6, 2023, DOI: 10.3390/en16062559.
6. Sathik M.H.M., Pou J., Prasanth S., Muthu V., Simanjorang R., Gupta A.K., *Comparison of IGBT junction temperature measurement and estimation methods-a review*, [In:] Asian Conference on Energy, Power and Transportation Electrification (ACEPT), 2017, DOI: 10.1109/ACEPT.2017.8168600.
7. Minkina W., *Theoretical basics of radiant heat transfer--practical examples of calculation for the infrared (IR) used in infrared thermography measurements*, "Quantitative InfraRed Thermography Journal", Vol. 18, No. 4, 2021, 269–282, DOI: 10.1080/17686733.2020.1738164.
8. Dziarski K., Hulewicz A., Skrzypczak S., *Indirect thermographic die temperature measurement of a SiC-based semiconductor diode under the conditions of natural and forced convection*, "Quantitative InfraRed Thermography Journal", Vol. 22, No. 3, 2024, 210–234, DOI: 10.1080/17686733.2024.2360254.
9. Rabczuk T., Xiao S.P., Sauer M., *Coupling of mesh-free methods with finite elements: basic concepts and test results*, "Communications in Numerical Methods in Engineering", Vol. 22, No. 10, 2006, 1031–1065, DOI: 10.1002/cnm.871.
10. Kawor E.T., Mattei S., *Emissivity measurements for Nextel Velvet Coating 811-21 between –36 °C and 82 °C*, [In:] 15th European Conference on Thermophysical Properties, Vol. 33, 551–556, DOI: 10.1068/htwu385.
11. Baillis D., Coquard R., Randrianalisoa J., Dombrovsky L., Viskanta R., *Thermal radiation properties of highly porous cellular foams*, "Special Topics & Reviews in Porous Media: An International Journal", Vol. 4, No. 2, 2013, 111–136, DOI: 10.1615/SpecialTopicsRevPorousMedia.v4.i2.20.
12. Feng S.Z., Cui X.Y., Li G.Y., *Transient thermal mechanical analyses using a face-based smoothed finite element method (FS-FEM)*, "International Journal of Thermal Sciences", Vol. 74, 2013, 95–103, DOI: 10.1016/j.ijthermalsci.2013.07.002
13. Dziarski K., Hulewicz A., Dombek G., Drużyński Ł., *Indirect Thermographic Temperature Measurement of a Power--Rectifying Diode Die*, "Energies", Vol. 15, No. 9, 2022, DOI: 10.3390/en15093203.
14. Mingxing T., Quoc V.L., *EfficientNet: Rethinking Model Scaling for Convolutional Neural Networks*, International Conference on Machine Learning ICML 2019, DOI: 10.48550/arXiv.1905.11946.
15. Taye M.M., *Theoretical Understanding of Convolutional Neural Network: Concepts, Architectures, Applications, Future Directions*, "Computation", Vol. 11, No. 3, 2023 DOI: 10.3390/computation11030052.

Other sources

16. JEDEC, *Global Standards for the Microelectronics Industry* [www.jedec.org/standards-documents/docs/jesd-51-1].
17. Electronic Components Datasheet Search, [www.alldatasheet.com/datasheet-pdf/pdf/1669893/WOLFSPEED/C2M0280120D.html].
18. TME, *Platinum Temperature Sensor Pt 1000-550*, [www.tme.eu/Document/67cf717905f835bc5efcdcd-56ca3a8e2/Pt1000-550_EN.pdf].
19. TME, *Thermally conductive adhesive*, [www.tme.eu/Document/7a228d9a81f73f75b-ba8707a2357bb2d/WLK_DTE].
20. Technical Data FLIR E50 (incl. Wi-Fi), [https://docs.rs-online.com/ca3e/0900766b81371810.pdf].
21. *User's manual FLIR Exx series*, [www.geass.com/wp-content/uploads/filebase/flir/termocamere/e40-e50-e60_comuni/Manuale-termocamere-Flir-E40-E50-E60.pdf].
22. FLIR, [www.apliter.com/wp-content/uploads/2019/11/FLIR-Lente-IR-Ampliaci%C3%B3n-2x-Serie-A3xx-Ficha-t%C3%A9cnica.pdf].

23. Polytec, *IRS Calilux Smart Blackbody for Infrared Cameras*, [www.polytec.com/fileadmin/website/optical-systems/ir-technik/pdf/datenblatt-calilux-schwarzkoerperstrahler.pdf].
24. Siemens, *PLC Controller*, [https://docs.rs-online.com/4ed5/0900766b81397276.pdf].
25. Siemens, Simatic HMI, [https://static.rapidonline.com/pdf/543842_v1.pdf].

Weryfikacja temperatury struktury półprzewodnikowej tranzystora SiC na podstawie obrazowania termowizyjnego i uczenia maszynowego

Streszczenie: W artykule przedstawiono metodę automatycznej weryfikacji termogramów obudów tranzystorów. Umożliwia rozróżnienie tych, które przedstawiają strukturę półprzewodnikową o właściwej temperaturze od tych przedstawiających strukturę półprzewodnikową o niewłaściwej temperaturze. Metoda ta opiera się na pośrednim termograficznym pomiarze temperatury struktury półprzewodnikowej tranzystora. W pracy opisano metodykę pomiaru, która zapewnia wiarygodną ocenę temperatury struktury przewodnikowej struktury półprzewodnikowej tranzystora. Zaproponowana metoda bazuje na pracach symulacyjnych z wykorzystaniem Metody Elementów Skończonych (MES). W badaniach zastosowano tranzystor pracujący w trybie impulsowym (przełączanie z określoną częstotliwością). Przedstawiono również metodę wyznaczania współczynników niezbędnych do wykonania prac symulacyjnych. Dodatkowo artykuł zawiera algorytm analizy termogramów obudów badanych tranzystorów oraz wyniki tej analizy. W konsekwencji możliwe jest rozróżnienie tranzystorów ze strukturą półprzewodnikową o właściwej temperaturze od tranzystorów ze struktura półprzewodnikową w niewłaściwej temperaturze.

Słowa kluczowe: termografia, sztuczna sieć neuronowa, konwolucyjna sieć neuronowa

Arkadiusz Hulewicz, PhD Eng.
arkadiusz.hulewicz@put.poznan.pl
ORCID: 0000-0001-9342-7430

A graduate of the Faculty of Electrical Engineering at the Poznan University of Technology, where he has been employed since 2001. Currently an assistant professor and academic teacher in the Department of Metrology of Electronics and Light Technology. Author and co-author of 93 publications. His main scientific interests are metrology, the thermographic measurements, the bio--measurements and the biomedical engineering, the optoelectronics, as well as modeling and signal processing, especially the thermal modelling.

Krzysztof Dziarski, PhD Eng.
krzysztof.dziarski@put.poznan.pl
ORCID: 0000-0002-7877-4116

Assistant Professor at the Institute of Electric Power Engineering, Poznań University of Technology. He obtained a PhD in technical sciences with a specialization in electrical engineering, focusing on advanced methods of thermal diagnostics in electronic systems. His doctoral dissertation concerned the application of infrared thermography and numerical simulations to analyze heat dissipation in semiconductor components. His research interests include thermal management, thermographic diagnostics, and reliability analysis of electronic components. He actively participates in scientific projects and teaching activities, supervising engineering and master's theses in the field of temperature measurement techniques, electronics, and residential electrical installations.